Check for updates

International Journal of Mechanical System Dynamics

WILEY

IJMSD International Journal of Mechanical System Dynamics Open Access

RESEARCH ARTICLE OPEN ACCESS

Robust Position Control of an Electro-Hydraulic Actuator via Metaheuristic Optimization of a Fractional-Order PID Controller

Ridvan Firat Cinar[1] | Davut Izci[2] | Serdar Ekinci[3] | Mohammad Salman[4] | Mohammad Al-Rabayah[4] | Ali Akdagli[5] | Ali Yildiz[5] | Filiz Karaomerlioglu[5] | Gökhan Yüksek[6]

[1]Department of Computer Engineering, Batman University, Batman, Turkey | [2]Department of Electrical and Electronic Engineering, Bursa Uludag University, Bursa, Turkey | [3]Department of Computer Engineering, Bitlis Eren University, Bitlis, Turkey | [4]College of Engineering and Technology, American University of the Middle East, Egaila, Kuwait | [5]Department of Electrical and Electronics Engineering, Mersin University, Mersin, Turkey | [6]Department of Electrical and Electronics Engineering, Batman University, Batman, Turkey

Correspondence: Davut Izci (davutizci@uludag.edu.tr)

Received: 21 February 2026 | **Revised:** 9 April 2026 | **Accepted:** 12 April 2026

Keywords: FOPID controller | four-way electro-hydraulic valve system | Kirchhoff's law algorithm | robustness | transient response

ABSTRACT

In this study, a robust position control strategy is presented for a two-stage electro-hydraulic actuator system using a fractional-order proportional–integral–derivative (FOPID) controller tuned by Kirchhoff's law algorithm (KLA). Electro-hydraulic systems exhibit strong nonlinearities, parameter uncertainties, and external disturbances, making accurate position control challenging. Classical integer-order controllers such as PI and PID often provide limited flexibility in shaping transient dynamics under such conditions, leading to performance degradation when system parameters vary. Although advanced nonlinear and adaptive control strategies can improve robustness, their implementation complexity and tuning burden may restrict their practical applicability. In addition, many existing metaheuristic-based tuning approaches rely on algorithm-specific parameters and may exhibit inconsistent convergence behavior across different operating conditions. To address these limitations, a control-oriented mathematical model of the electro-hydraulic positioning system is first derived from linearized valve flow relations, actuator continuity equations, and load dynamics, and a reduced-order transfer function preserving the dominant behavior is obtained for controller design. The FOPID controller is adopted to enlarge the tuning space through fractional integral and derivative orders, enabling finer dynamic shaping than classical integer-order structures. The controller parameters are determined automatically by formulating a multi-term time-domain objective function that penalizes overshoot, settling time, and accumulated tracking error. The KLA metaheuristic, inspired by electrical circuit laws, is employed to solve this constrained optimization problem without introducing algorithm-specific control parameters. Under identical optimization settings (population size 25, 40 iterations, 20 independent runs), the proposed KLA approach achieves the best statistical performance among the tested optimizers, with a minimum fitness value of 1.2511, mean value of 1.2881, and standard deviation of 0.0258, outperforming APO, PSO, and DE according to Wilcoxon signed-rank tests ($p \approx 8.86 \times 10^{-5}$). For a 20 cm step command, the KLA-tuned FOPID controller yields a rise time of 0.1664 s, settling time of 0.3034 s, overshoot of 0.0124%, and IAE of 1.5244 cm·s, improving all metrics relative to both competing optimizers and KLA-tuned PI, PIDF, and 2-DOF PID controllers. Additional simulations demonstrate stable and accurate tracking under multi-level and time-varying references, parametric variations from −10% to +25%, and combined disturbance and measurement noise. The results indicate that the KLA-based FOPID design provides a fast, accurate, and robust control solution for electro-hydraulic positioning systems.

This is an open access article under the terms of the Creative Commons Attribution License, which permits use, distribution and reproduction in any medium, provided the original work is properly cited.

© 2026 The Author(s). *International Journal of Mechanical System Dynamics* published by John Wiley & Sons Australia, Ltd on behalf of Nanjing University of Science and Technology.

1 | Introduction

Electro-hydraulic actuator systems are widely employed in industrial automation, heavy machinery, aerospace platforms, and precision motion applications because of their high power density, rapid response capability, and suitability for severe operating environments [1–4]. Despite these advantages, accurate position control of electro-hydraulic systems remains difficult in practice due to strong nonlinearities, parameter uncertainty, fluid compressibility, valve-flow nonlinear behavior, and external disturbances [5–8]. Variations in load, leakage, pressure dynamics, and valve characteristics often degrade closed-loop performance and reduce the reliability of controllers designed under nominal assumptions. For this reason, the development of control strategies that combine high transient performance with practical robustness continues to be an important research problem.

From the viewpoint of controller structure, a broad range of methods has been reported for electro-hydraulic systems. In addition to classical linear feedback designs, nonlinear and adaptive control schemes have been introduced to better address the severe dynamic characteristics of such plants. A higher-order nonlinear model combined with sliding-mode control was reported for hydraulic pressure regulation in electro-hydraulic brake systems in Ref. [9], where fast tracking and strong disturbance rejection were achieved under varying operating conditions. Robust adaptive fuzzy backstepping control for an electro-hydraulic servo position system was investigated in Ref. [10], while disturbance-observer-supported nonlinear control design for electro-hydraulic servo systems was examined in Ref. [11]. These studies demonstrate that advanced nonlinear control structures can provide strong tracking capability and robustness. However, their mathematical complexity, implementation burden, and parameter-adjustment difficulty may limit their attractiveness in many engineering settings where a simpler yet still flexible controller is preferred.

Alongside these advanced nonlinear schemes, PID-type controllers remain attractive because of their transparency, interpretability, and ease of implementation. Nevertheless, classical PI and PID structures may provide insufficient flexibility when the plant exhibits memory effects, nonlinear transients, or significant operating-point variation. This limitation has motivated the use of fractional-order PID (FOPID) control, in which the integral and derivative orders are allowed to take non-integer values [12–14]. By enlarging the controller design space beyond the conventional integer-order form, FOPID control enables finer shaping of the transient and frequency responses. A recent electro-hydraulic tracking study in Ref. [13] showed that an optimized FOPID controller can improve tracking performance relative to classical controllers, which supports the suitability of fractional-order structures for hydraulic actuation problems.

The rationale for selecting a fractional-order controller has also been strengthened in recent years by the emergence of nonlinear and augmented FOPID variants. For example, a softsign-based FOPID controller was recently proposed for magnetic levitation control, where the smooth bounded nonlinearity was used to moderate abrupt control action while preserving the flexibility of fractional dynamics [15]. Similarly, a sigmoid-based FOPID controller was introduced for automatic voltage regulator systems, where improved robustness and dynamic performance were reported relative to both classical FOPID and nonlinear integer-order alternatives [16]. These developments indicate that the fractional-order framework is not only a direct extension of PID, but also a structurally fertile platform capable of being enriched by smooth nonlinear mappings when stronger transient shaping is required. In this context, the present study adopts the standard FOPID architecture as a principled middle ground: it retains the conceptual simplicity of PID-type control while offering richer dynamic adjustability than conventional integer-order structures, without introducing the additional structural complexity associated with more elaborate nonlinear augmentations.

A second research stream concerns the optimization and tuning methodologies used for electro-hydraulic systems. Since electro-hydraulic parameter identification and controller design are commonly associated with multimodal and nonconvex search spaces, many studies have formulated the tuning task as an optimization problem. Improved particle swarm optimization (PSO) was used in Ref. [17] for identifying electro-hydraulic system parameters under challenging operating conditions, and chaos-enhanced metaheuristics were employed in Ref. [18] for electro-hydraulic parameter estimation with improved global search ability. More generally, metaheuristic algorithms such as PSO, differential evolution (DE), and related nature-inspired methods have been widely used for PID and FOPID tuning because gradient information is not required and complex search domains can be handled effectively [19–22]. However, many such optimizers rely on several algorithm-specific coefficients, and their convergence characteristics may vary significantly with the problem class and parameter setting.

Recently, attention has also been directed toward new PID variants that extend the classical structure through nonlinear mappings, intelligent learning, or biologically inspired adaptation. Examples include the Gudermannian PID controller, where a smooth, bounded Gudermannian transformation is embedded into the PID framework to improve transient shaping [23]; BELBIC-PID controllers, where emotional-learning mechanisms are coupled with PID action for data-driven control tasks [24]; CMAC-PID controllers, where cerebellar-model-based learning is used to adapt or support PID gains [25]; and neuroendocrine-PID controllers, where endocrine-inspired adaptation is incorporated into the control law [26]. These approaches are intellectually interesting and, in several applications, have been shown to improve performance over standard PID designs. However, they typically introduce additional nonlinear mappings, adaptive subsystems, memory structures, or data-driven learning mechanisms that increase controller complexity, enlarge the number of design choices, and may require problem-specific calibration or training. By contrast, the present work does not pursue a learning-augmented or biologically inspired PID architecture. Instead, it investigates whether a FOPID structure, tuned in a fully optimization-driven manner, can provide a more favorable balance between structural simplicity, tuning flexibility, and robust electro-hydraulic position-control performance.

From this perspective, a clear research gap can be identified. Although electro-hydraulic actuator systems have been studied using nonlinear control laws, adaptive schemes, and metaheuristic

27671402, 0, Downloaded from https://onlinelibrary.wiley.com/doi/10.1002/msd2.70076 by Turkey Cochrane Evidence Aid, Wiley Online Library on [04/09/2026]. See the Terms and Conditions (https://onlinelibrary.wiley.com/terms-and-conditions) on Wiley Online Library for rules of use; OA articles are governed by the applicable Creative Commons License

tuning approaches, the literature remains limited in terms of studies that jointly address:

i. a control-oriented electro-hydraulic actuator model suitable for optimization-based design,

ii. simultaneous tuning of both gains and fractional orders of a FOPID controller,

iii. use of a non-parametric physics-inspired optimizer with low algorithmic adjustment burden, and

iv. a structured comparison not only against alternative optimizers but also against alternative PID-type controller architectures under identical settings. In particular, while KLA has shown promising optimization capability on benchmark problems [27], its suitability for fractional-order controller tuning in electro-hydraulic position control has not been systematically examined.

Motivated by these observations, a KLA-based FOPID control framework is developed in this study for robust position control of a two-stage electro-hydraulic actuator system. A control-oriented mathematical model is first constructed using linearized valve flow relations, actuator continuity equations, and mechanical load dynamics. A reduced second-order plant model preserving dominant dynamics is then derived for controller design and optimization. A FOPID controller is adopted to enlarge the tuning space through fractional integral and derivative orders. Controller parameters are obtained automatically by solving a constrained optimization problem in which a composite time-domain objective function combining percent overshoot (OS), settling time, and integral absolute error (IAE) is minimized using the KLA.

The effectiveness of the proposed tuning framework is evaluated through extensive simulation studies and compared with several widely used metaheuristic optimizers, namely artificial protozoa optimizer (APO) [28], PSO [29], and DE [30], under identical computational settings. Statistical analyses over 20 independent runs are performed, including dispersion metrics and Wilcoxon signed-rank significance tests. The KLA-based design achieves the best minimum fitness value of 1.2511, the lowest mean value of 1.2881, and the smallest standard deviation (SD) of 0.0258 among all tested optimizers. In step tracking of a 20 cm position command, the KLA-tuned FOPID controller yields a rise time of 0.1664 s, a settling time of 0.3034 s, an overshoot of 0.0124%, and an IAE of 1.5244 cm·s, outperforming the competing tuning approaches.

To separate the influence of controller structure from tuning algorithm effects, KLA-based tuning is also applied to PI [31], filtered PID [32], and two-degree-of-freedom PID [33] controllers. Comparative results indicate that the fractional-order controller structure provides faster settling and lower accumulated error under the same optimization framework. Robustness is further examined through variable setpoint tracking, structured parametric variations from −10% to +25%, and combined disturbance and measurement noise scenarios, where stable operation with acceptable performance degradation is observed.

The remainder of the paper is organized as follows. Section 2 presents the electro-hydraulic system modeling procedure and the reduced plant representation. Section 3 describes the KLA method, the FOPID controller structure, and the optimization formulation. Section 4 reports the statistical and time-domain comparative results. Section 5 investigates robustness under parametric variations, disturbances, and noise. Final conclusions are given in Section 6.

2 | System Modeling of the Electro-Hydraulic Positioning System

The plant considered in this study is a two-stage electro-hydraulic positioning system composed of an electro-hydraulic valve, a double-acting single-rod linear actuator, and a translational mechanical load. As illustrated in Figure 1, the valve section regulates the hydraulic flow delivered to the actuator chambers, whereas the actuator transforms the resulting pressure difference into translational motion of the load [34]. The controlled output is the actuator displacement z_{out}, and the displacement signal is measured through the feedback transducer with gain h. The control-oriented block representation corresponding to this arrangement is shown in Figure 2. The mathematical model is constructed from the linearized valve-flow relations, actuator continuity equation, hydraulic pressure–force conversion, and mechanical load dynamics. The model parameters used throughout the derivation are listed in Table 1.

For the critically centered four-way valve operated around its nominal point, the load flow can be linearized with respect to the main spool displacement and the pressure difference across the actuator chambers. Accordingly, the load-flow relation may be written as $Q_L = 2K_q x_m - K_c(P_A|P_B)$ where Q_L denotes the load flow, x_m is the main spool displacement, K_q is the flow gain of the control valve, and K_c is the pressure-flow coefficient [34]. The pressures P_A and P_B correspond to the two actuator chambers shown in Figure 1. Under the incompressible-fluid assumption and neglecting leakage, the flow entering the actuator is related to the piston velocity through the continuity equation, $Q_L = A\dot{z}_{\text{out}}$, where A is the effective piston area and z_{out} is the actuator displacement.

By combining Equations (1) and (2), the pressure difference between the two sides of the actuator can be expressed as follows [34].

$$P_A - P_B = \frac{2K_q}{K_c}x_m - \frac{A}{K_c}\dot{z}_{\text{out}} \tag{1}$$

This relation shows that the chamber pressure difference is governed jointly by the spool displacement and the actuator velocity. Therefore, the hydraulic subsystem introduces both an input-dependent driving term and a velocity-dependent damping contribution.

The two-stage valve shown in Figure 1 is represented in Figure 2 by an equivalent first-order block. The relation between the

27671402, 0, Downloaded from https://onlinelibrary.wiley.com/doi/10.1002/msd2.70076 by Turkey Cochrane Evidence Aid, Wiley Online Library on [04/09/2026]. See the Terms and Conditions (https://onlinelibrary.wiley.com/terms-and-conditions) on Wiley Online Library for rules of use; OA articles are governed by the applicable Creative Commons License

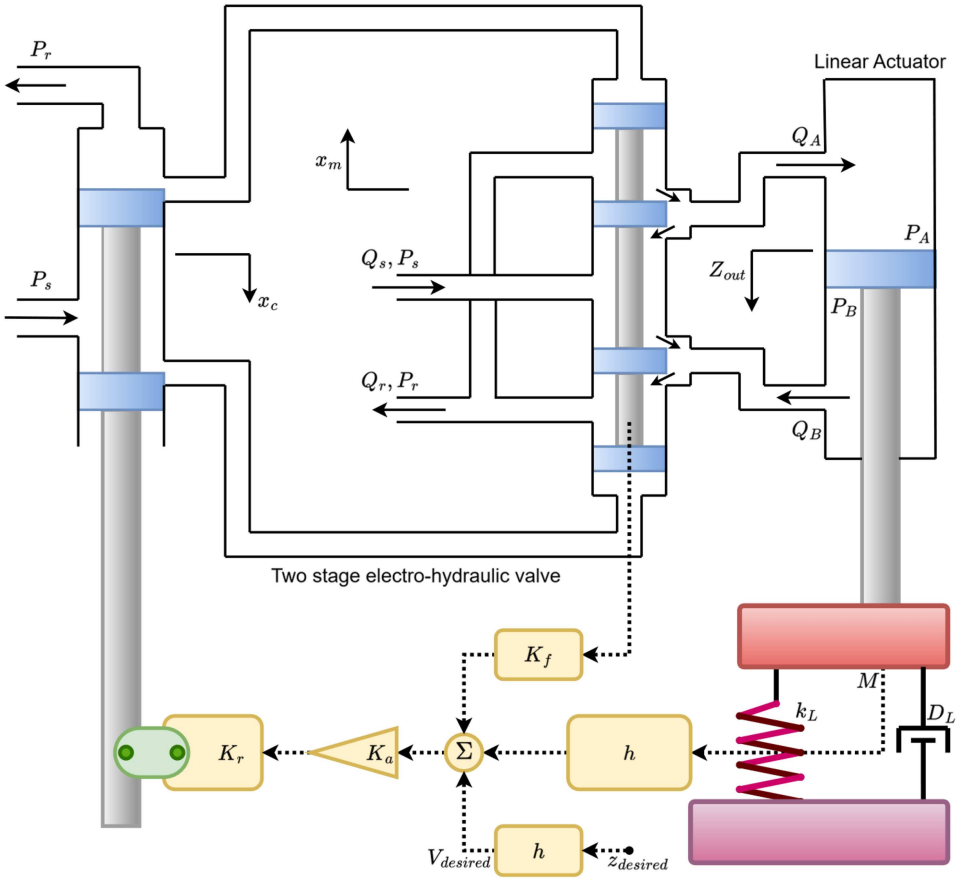


FIGURE 1 | The schematic diagram of the electro-hydraulic translational system.

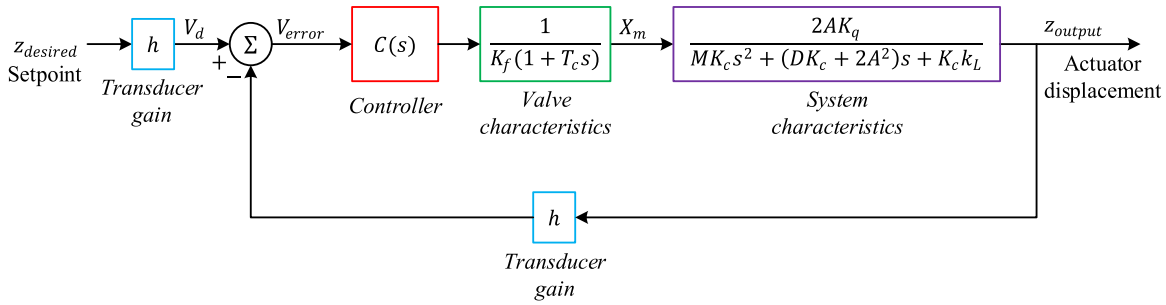


FIGURE 2 | Translational system block diagram.

valve-control signal $V_c(s)$ and the main spool displacement $X_m(s)$ is written as [34]:

$$\frac{X_m(s)}{V_c(s)} = \frac{1}{K_f(1 + T_v s)} \tag{2}$$

where K_f is the main spool feedback transducer gain and T_c is the valve time constant given by Equation (4) [34].

$$T_c = \frac{A_m}{K_a K_f K_r} \tag{3}$$

Here, A_m denotes the main spool area, K_a is the proportional control gain of the valve stage, and K_r is the ratio between the input voltage and the control spool displacement. The first-order form in equation corresponds to the valve-characteristics block shown in Figure 2.

The actuator drives a translational load modeled as a mass–spring–damper system, as depicted in Figure 1. By applying Newton's law, the mechanical load dynamics can be written as $M\ddot{z}_{\text{out}} + D_L\dot{z}_{\text{out}} + k_L z_{\text{out}} = F_L$ where M is the load mass, D_L is the viscous damping coefficient, k_L is the load spring stiffness, and F_L is the hydraulic force acting on the piston.

27671402, 0, Downloaded from https://onlinelibrary.wiley.com/doi/10.1002/msd2.70076 by Turkey Cochrane Evidence Aid, Wiley Online Library on [04/09/2026]. See the Terms and Conditions (https://onlinelibrary.wiley.com/terms-and-conditions) on Wiley Online Library for rules of use; OA articles are governed by the applicable Creative Commons License

TABLE 1 | Parameters of hydraulic system [34, 35].

Parameter	Definition	Value	Unit
K_q	Flow gain of control valve	0.359	m^2/s
K_c	Pressure-flow coefficient	1.7×10^{-11}	$m^3/Pa/s$
A_m	Main spool area	550×10^{-6}	m^2
M	Load mass	1	kg
A	Actual piston area	1.1×10^{-3}	m^2
K_a	Proportional control gain	1	–
K_f	Main spool feedback transducer gain	1	–
K_r	Ratio between input voltage and control spool displacement	1	–
D	Load damping	1	N·s/m
k_L	Load spring stiffness	1	N/m
h	Transducer gain	1	–

For an ideal actuator, the hydraulic force is proportional to the chamber pressure difference, that is $F_L = A(P_A|P_B)$ [34]. Substituting Equation (1) into the latter definition gives:

$$F_L = \frac{2AK_q}{K_c}x_m - \frac{A^2}{K_c}\dot{z}_{\text{out}} \times 2 \tag{4}$$

which yields the definition given by Equation (5).

$$F_L = \frac{2AK_q}{K_c}x_m - \frac{2A^2}{K_c}\dot{z}_{\text{out}} \tag{5}$$

By substituting Equation (5) into $M\ddot{z}_{\text{out}} + D_L\dot{z}_{\text{out}} + k_L z_{\text{out}} = F_L$, the actuator-load dynamics become as follows.

$$M\ddot{z}_{\text{out}} + \left(D_L + \frac{2A^2}{K_c}\right)\dot{z}_{\text{out}} + k_L z_{\text{out}} = \frac{2AK_q}{K_c}x_m \tag{6}$$

Taking the Laplace transform of Equation (6) under zero initial conditions gives

$$\left[Ms^2 + \left(D_L + \frac{2A^2}{K_c}\right)s + k_L\right]Z_{\text{out}}(s) = \frac{2AK_q}{K_c}X_m(s) \tag{7}$$

Equation (7) corresponds to the actuator-side system-characteristics block in Figure 2. It is observed that the hydraulic coupling contributes an additional damping term, $2A^2/K_c$, to the mechanical subsystem. By cascading the valve relation in Equation (2) with the actuator dynamics in Equation (7), the transfer function from the valve-control signal $V_c(s)$ to the actuator displacement $Z_{\text{out}}(s)$ is obtained as follows.

$$G_{\text{plant}}(s) = \frac{Z_{\text{out}}(s)}{V_c(s)} = \frac{2AK_q}{K_f(1 + T_c s)(MK_c s^2 + (DK_c + 2A^2)s + K_c k_L)} \tag{8}$$

This expression provides the complete control-oriented linear model of the electro-hydraulic positioning system. The numerical values of the model parameters are taken from Table 1. These parameters correspond directly to the physical quantities indicated in Figure 1 and to the blocks appearing in Figure 2. In particular, K_q, K_c, A_m, A, K_a, K_f, and K_r characterize the valve and hydraulic conversion mechanism, whereas M, D, and k_L describe the mechanical load. After substituting the parameter values from Table 1 into the complete transfer function in Equation (8), the resulting forward-path model becomes as follows [34].

$$G(s) = \frac{3.03 \times 10^{10}}{s^3 + 1.4235 \times 10^5 s^2 + 653s + 7.02 \times 10^{-5}} \tag{9}$$

Inspection of this model shows that one pole is located far from the dominant dynamics. Following the standard reduction procedure, this fast pole can be neglected without materially affecting the dominant transient behavior. This simplification leads to the reduced form given in Equation (10) [34].

$$G_{\text{plant}}(s) = \frac{213,041}{s^2 + 653s} \tag{10}$$

The reduced model in Equation (10) is adopted in the subsequent controller-design and optimization stages. This approximation preserves the dominant behavior of the electro-hydraulic positioning system while providing a simpler and more convenient representation for closed-loop synthesis. In this way, the essential valve–actuator dynamics reflected in Figure 1 and summarized in Figure 2 are retained, whereas the unnecessary high-frequency component is removed from the control-design model.

3 | Proposed Approach

3.1 | Overview of Kirchhoff's Law Algorithm (KLA)

KLA is a physics-inspired, population-based meta-heuristic that reformulates the optimization process through an analogy with resistive electrical circuits [27]. In this framework, each candidate solution is represented as a node in an equivalent circuit,

27671402, 0, Downloaded from https://onlinelibrary.wiley.com/doi/10.1002/msd2.70076 by Turkey Cochrane Evidence Aid, Wiley Online Library on [04/09/2026]. See the Terms and Conditions (https://onlinelibrary.wiley.com/terms-and-conditions) on Wiley Online Library for rules of use; OA articles are governed by the applicable Creative Commons License

and its position in the search space is interpreted as a nodal voltage. The objective function value associated with a solution determines the electrical characteristics of the network, most notably the resistances between nodes. Consequently, the collective dynamics of the population are governed by the same principles that regulate current flow in physical circuits, namely Ohm's law and Kirchhoff's current law (KCL).

Let $X_i \in \mathbb{R}^D$ denote the position of the i-th solution ($i = 1, ..., N_{pop}$) and $f(X_i)$ its objective value. In the electrical analogy, X_i corresponds to a nodal voltage V_i. The interaction between two nodes i and j is modeled by a resistive branch whose resistance depends on their fitness values. The resistance is defined as:

$$R_{ij}^k = \frac{1}{(\text{rand} + \text{rand})} \left(\frac{f(X_i^k)}{f(X_j^k)} \right)^{2\,\text{rand}} \tag{11}$$

where rand $\in [0,1]$ is a uniformly distributed random number and k denotes the iteration index. This formulation ensures that solutions with superior objective values induce lower resistances, thereby attracting more "current" in the circuit sense.

According to Ohm's law, the current flowing between two nodes is proportional to the voltage difference and inversely proportional to the resistance. In KLA, this current is translated into a displacement in the search space. The total change in the position of node $i$is obtained by aggregating the currents contributed by three randomly selected nodes a, b, and c:

$$\Delta X_i^k = \sum_{j=a,b,c} \frac{X_i^k - X_j^k}{R_{ij}} = \sum_{j \in a,b,c} (\text{rand}_{1_j} + \text{rand}_{2_j}) \left(\frac{f\left(X_j^k\right)}{f\left(X_i^k\right)} \right)^{2 \times \text{rand}_{3_j}} \left(\frac{f\left(X_j^k\right) - f\left(X_i^k\right)}{\left| f\left(X_j^k\right) - f\left(X_i^k\right) \right| + \varepsilon} \right) \left(X_i^k - X_j^k\right) \tag{12}$$

where ε is a small positive constant preventing numerical singularities. The sign term regulates the direction of the current, enforcing motion from higher-resistance (inferior) nodes toward lower-resistance (superior) ones, in accordance with physical current flow. The nodal voltage, that is, the candidate solution, is then updated as $X_i^{k+1} = X_i^k + \Delta X_i^k$.

The aggregation of currents in Equation (12) reflects KCL, which states that the algebraic sum of currents entering a node is zero. In the optimization context, this principle guarantees that the influence of multiple population members is balanced at each update, preventing dominance by a single elite solution and preserving population diversity. Through this mechanism, KLA naturally orchestrates both exploration and exploitation.

During early iterations, random resistances and wide voltage differences promote extensive current redistribution, enabling broad exploration of the search space. As the algorithm progresses and superior solutions emerge, resistances concentrate around these regions, channeling currents toward promising areas and intensifying exploitation. The overall procedure begins with the random initialization of N_{pop} nodal voltages. At each iteration, objective values are evaluated, resistances are constructed, and nodal currents are computed through KCL-based interactions. Updated voltages are accepted when improvement is achieved, and the global best solution is continuously tracked. This loop is repeated until the termination criterion is satisfied. The working mechanism of KLA is provided in the flowchart depicted in Figure 3. By embedding the optimization dynamics within the physical laws of electrical circuits, KLA eliminates the need for explicit control parameters. The search trajectory is instead governed by self-regulated current redistribution, which inherently favors low-resistance (high-quality) pathways. This correspondence between energy minimization in circuits and cost minimization in optimization establishes KLA as a simple yet robust framework, capable of adaptively steering the population toward the global optimum while maintaining diversity across iterations.

3.2 | FOPID Controller

The FOPID controller is employed in this study as the main control structure due to its enhanced flexibility and improved robustness compared to the classical integer-order PID controller. In contrast to the conventional PID form, the orders of the integral and derivative operators are not restricted to unity but are treated as additional tuning parameters [36]. This extension enlarges the feasible controller design space and enables more precise shaping of the closed-loop dynamics. Detailed theoretical background and application-oriented discussions of FOPID control can be found in [36, 37]. The transfer function of the FOPID controller in the Laplace domain is expressed as:

$$C_{\text{FOPID}}(s) = \frac{U(s)}{E(s)} = K_p + \frac{K_i}{s^\lambda} + K_d s^\mu \tag{13}$$

where $E(s)$ denotes the error signal and $U(s)$ represents the controller output. The parameters K_p, K_i, and K_d are the proportional, integral, and derivative gains, respectively. The real-valued parameters λ and μ define the fractional orders of the integral and derivative actions. When $\lambda = 1$ and $\mu = 1$, the classical PID controller is recovered as a special case [37]. Similarly, appropriate selections of λ and μ reduce the structure to PI, PD, or P controllers, which indicates that the conventional controllers are embedded within the fractional-order framework.

The internal structure of the FOPID controller used in this work is illustrated in Figure 4. As shown in the figure, the error signal is processed through three parallel branches corresponding to proportional, fractional integral, and fractional derivative actions. The integral path includes a fractional operator $1/s^\lambda$, while the derivative path contains the fractional operator s^μ. The weighted outputs of these three branches are summed to generate the final control signal. This parallel configuration preserves the intuitive interpretation of PID-type control while introducing additional degrees of freedom through the fractional orders.

Fractional operators cannot be implemented directly in practical digital or analog control systems and therefore must be approximated by finite-dimensional rational transfer functions.

27671402, 0, Downloaded from https://onlinelibrary.wiley.com/doi/10.1002/msd2.70076 by Turkey Cochrane Evidence Aid, Wiley Online Library on [04/09/2026]. See the Terms and Conditions (https://onlinelibrary.wiley.com/terms-and-conditions) on Wiley Online Library for rules of use; OA articles are governed by the applicable Creative Commons License

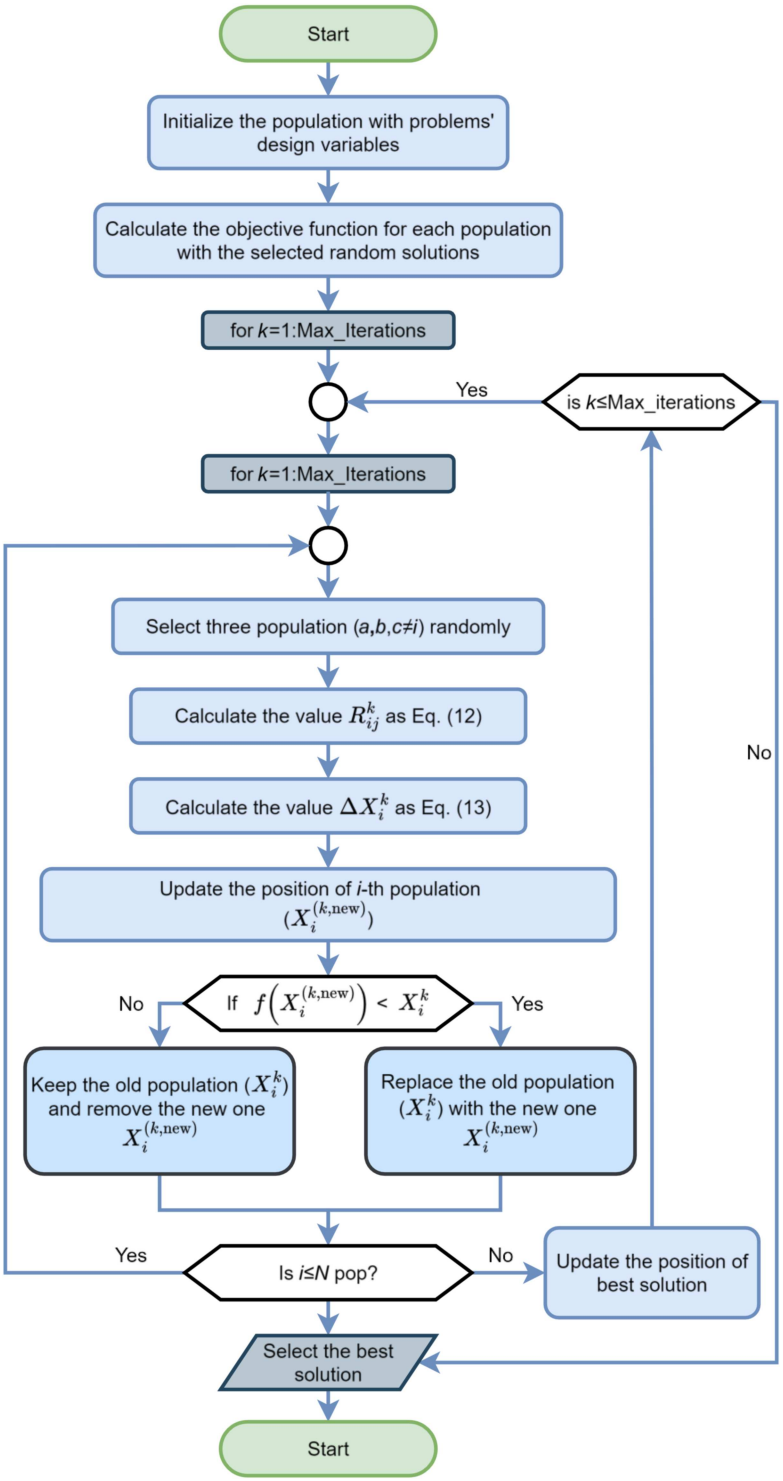


FIGURE 3 | Flowchart of KLA.

In practical implementations, frequency-domain approximation techniques are typically adopted to represent s^{α} operators over a specified frequency band [37]. Among available approaches, Oustaloup-type recursive approximations are widely used because they provide stable and accurate realizations using interlaced pole–zero distributions over the selected frequency interval [37]. By means of such approximations, the fractional integral and derivative terms are replaced by realizable high-order filters, allowing the FOPID controller to be implemented within standard simulation and control environments.

In the present study, the controller parameter vector is defined as $\Theta = \{K_p, K_i, K_d, \lambda, \mu\}$, and all five parameters are tuned simultaneously through the proposed KLA-based optimization procedure described in the following subsection. This formulation allows both gain levels and fractional orders to be

27671402, 0, Downloaded from https://onlinelibrary.wiley.com/doi/10.1002/msd2.70076 by Turkey Cochrane Evidence Aid, Wiley Online Library on [04/09/2026]. See the Terms and Conditions (https://onlinelibrary.wiley.com/terms-and-conditions) on Wiley Online Library for rules of use; OA articles are governed by the applicable Creative Commons License

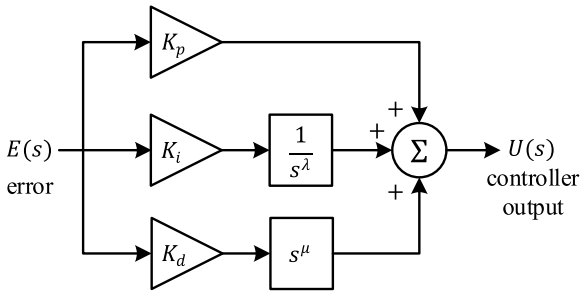


FIGURE 4 | Block diagram of FOPID controller.

adapted to the electro-hydraulic plant dynamics, thereby improving transient performance and robustness characteristics relative to fixed-order controllers.

3.3 | KLA-Based Optimization Problem

In this study, the parameters of the FOPID controller are determined through an automatic tuning procedure based on the KLA. The tuning task is formulated as a constrained optimization problem in which the controller parameter vector is adjusted to achieve improved transient performance of the electro-hydraulic positioning system described in Section 2. The optimization loop couples the candidate FOPID controller with the hydraulic plant model, evaluates the closed-loop response, and updates the controller parameters iteratively using the KLA search mechanism. The controller synthesis in this study is performed under several design assumptions that are introduced to maintain a control-oriented and computationally tractable formulation. First, the electro-hydraulic actuator is represented by the reduced second-order model derived in Section 2, which preserves the dominant dynamics of the original system and is therefore adopted as the basis for controller tuning. Second, a unity-feedback control structure is considered throughout the optimization stage, and the controller is designed for reference tracking under a prescribed step input. Third, the fractional-order operators are understood in their practical approximated form, as discussed in Section 3.2, so that the optimized controller remains compatible with standard realizable implementations. These assumptions do not alter the physical meaning of the problem, but they provide a consistent framework for optimization-based controller synthesis.

The decision vector to be optimized is defined as $\Theta = \{K_p, K_i, K_d, \lambda, \mu\}$, where K_p, K_i, and K_d denote the proportional, integral, and derivative gains, and λ and μ represent the fractional integral and derivative orders, respectively. For each candidate parameter set generated by KLA, a closed-loop simulation of the hydraulic system is performed, and the time-domain response is evaluated. To quantify the control performance, a composite objective (fitness) function is defined as:

$$F_{\text{fit}} = \gamma_1 \cdot OS + \gamma_2 \cdot t_s + (1 - \gamma_1 - \gamma_2) \cdot \int_0^{t_{\text{sim}}} e(t)\mathrm{d}t \quad (14)$$

where OS is the percent overshoot, t_s is the settling time defined with respect to the $\pm 2\%$ tolerance band, and $e(t)$ is the instantaneous tracking error. The term t_{sim} denotes the total simulation duration. In this work, the weight factors are selected as $\gamma_1 = \gamma_2 = 0.1$, and the simulation horizon is taken as $t_{\text{sim}} = 2\,\text{s}$. With this formulation, a balanced compromise is enforced between overshoot reduction, fast settling, and overall error suppression. The integral error term ensures that the entire transient behavior contributes to the performance index rather than only peak-based metrics. During the evaluation of the fitness function, a reference step change corresponding to a 20 cm actuator displacement setpoint applied at $t = 0$ is considered. All candidate controllers are therefore assessed under identical operating conditions, ensuring fair comparison of transient characteristics. The search ranges assigned to the FOPID parameters are given in Table 2. These bounds are selected to remain consistent with practical controller magnitudes while providing sufficient freedom for fractional-order tuning. Both gain parameters and fractional orders are included within the optimization domain so that KLA can jointly adjust controller strength and dynamic shaping capability. The bounds given in Table 2 also define the design constraints of the controller-synthesis problem. These constraints are imposed to avoid nonphysical or excessively aggressive parameter combinations and to keep the controller within a practically meaningful operating region. In particular, the gain limits restrict the overall control effort to a numerically reasonable interval, while the bounds on the fractional orders preserve the intended fractional-order character of the controller without allowing degenerate or excessively high-order behavior. Accordingly, the optimization problem may be interpreted as the search for the parameter vector $\theta = [K_p, K_i, K_d, \lambda, \mu]$ that minimizes the performance index in Equation (15) subject to the lower and upper bounds listed in Table 2.

The overall optimization structure is illustrated in Figure 5. As shown in the figure, an initial population of candidate FOPID parameter sets is first generated within the prescribed bounds. For each candidate, the closed-loop system composed of the FOPID controller and the hydraulic plant is simulated, and the fitness value in Equation (15) is computed. These fitness values are then supplied to the KLA module, where parameter updates are produced according to the circuit-inspired search rules described in Section 3.1. The updated parameter sets are re-evaluated through the same simulation-based procedure, and the best admissible solution is retained through the iterative search process. In this framework, the controller synthesis proceeds by repeatedly evaluating closed-loop behavior, rejecting inferior parameter combinations through the objective-based comparison mechanism, and steering the search toward parameter sets that provide improved transient performance.

From the standpoint of stability and admissibility, the proposed design procedure relies on closed-loop simulation and performance-based screening rather than on an explicit

TABLE 2 | Bounds of FOPID controller parameters.

Bounds	K_p	K_i	K_d	λ	μ
Lower	0.01	0.0001	0.00005	0.5	0.5
Upper	0.04	0.0008	0.00040	1.5	1.5

27671402, 0, Downloaded from https://onlinelibrary.wiley.com/doi/10.1002/msd2.70076 by Turkey Cochrane Evidence Aid, Wiley Online Library on [04/09/2026]. See the Terms and Conditions (https://onlinelibrary.wiley.com/terms-and-conditions) on Wiley Online Library for rules of use; OA articles are governed by the applicable Creative Commons License

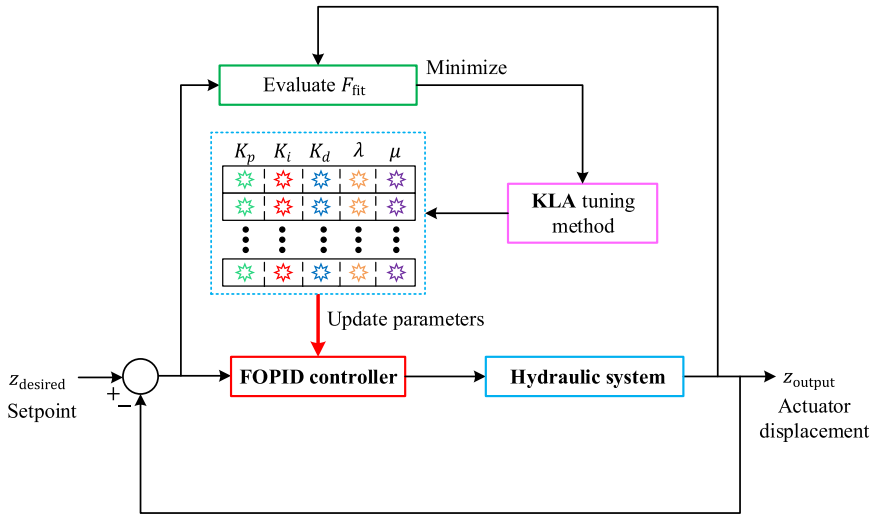


FIGURE 5 | The optimization procedure of the KLA-based FOPID controller for hydraulic system.

analytical stability derivation. Since the tuning task is carried out on the reduced control-oriented model and the objective function penalizes unfavorable transient behavior through overshoot, settling time, and accumulated error, parameter sets that do not yield acceptable closed-loop responses are naturally disfavored during the optimization process. Therefore, the final controller is obtained as the best constrained solution within the admissible search domain under the adopted closed-loop performance criteria.

From a closed-loop stability perspective, the proposed design is interpreted in a control-oriented local sense that is consistent with the reduced plant model adopted in Section 2. After the fractional integral and derivative operators are represented through standard finite-dimensional rational approximation, the FOPID-controlled system may be viewed as an equivalent finite-dimensional closed-loop dynamic system. Under this representation, closed-loop stability is associated with the admissibility of the controller parameter vector and with the requirement that the closed-loop response remain bounded and converge toward the reference under the prescribed operating conditions. Accordingly, the present synthesis framework does not rely on a separate Lyapunov-function construction for the full nonlinear hydraulic system; instead, stability is justified through the combination of model reduction, bounded controller constraints, and simulation-based admissibility screening within the optimization loop. More specifically, the parameter bounds in Table 2 restrict the search to a practically meaningful controller domain, while the objective function in Equation (15) penalizes excessive overshoot, prolonged settling, and large accumulated tracking error. As a consequence, controller candidates that lead to oscillatory, weakly damped, or otherwise unacceptable closed-loop behavior are disfavored during the optimization process. The final optimized controller is therefore selected from among the admissible parameter sets that produce bounded and well-settled closed-loop responses for the adopted reference-tracking problem. In this sense, the proposed design ensures practical closed-loop stability of the reduced electro-hydraulic model under the considered operating conditions, and this conclusion is further supported by the nominal and robustness results reported in Sections 4 and 5, where no unstable response is observed for the retained controller solution.

4 | Simulation Results

To ensure a clear and consistent evaluation framework, the performance of the proposed and comparative control approaches is assessed using a set of standard time-domain and statistical performance criteria. The primary transient-response metrics include rise time (t_r), settling time (t_s) defined with respect to the $\pm 2\%$ tolerance band, and OS which collectively characterize the speed and damping behavior of the closed-loop system. From an optimization perspective, the composite objective (fitness) function defined in Equation (15), which combines overshoot, settling time, and integral error components, serves as the primary performance index for algorithm comparison. Furthermore, statistical indicators including minimum, maximum, mean, and SD of the fitness values across multiple independent runs are used to evaluate the consistency and reliability of each optimization method. These criteria provide a comprehensive basis for comparing both the optimization performance and the closed-loop control behavior in the following subsections.

4.1 | Statistical Analysis

In order to evaluate the effectiveness and reliability of the proposed KLA-based FOPID tuning strategy, a statistical performance analysis was conducted and compared with three widely used metaheuristic optimizers: APO [28], PSO [29], and DE [30]. All algorithms were executed under identical experimental conditions to ensure a fair comparison. For each method, 20 independent runs were performed with a population size of 25 and a maximum iteration number of 40. The fitness function defined in Equation (15) was used as the performance index in all runs.

The distribution of fitness values obtained across 20 runs is illustrated in Figure 6. It is observed that the proposed KLA method

27671402, 0, Downloaded from https://onlinelibrary.wiley.com/doi/10.1002/msd2.70076 by Turkey Cochrane Evidence Aid, Wiley Online Library on [04/09/2026]. See the Terms and Conditions (https://onlinelibrary.wiley.com/terms-and-conditions) on Wiley Online Library for rules of use; OA articles are governed by the applicable Creative Commons License

consistently produces lower fitness values compared to APO, PSO, and DE in most runs. Moreover, the spread of the KLA results appears narrower, indicating improved repeatability and reduced sensitivity to random initialization. In contrast, the competing methods exhibit larger fluctuations between runs, especially PSO and DE, where higher worst-case values are recorded.

A more detailed statistical summary is provided in Table 3, where the minimum, maximum, mean, and SD of the fitness values are reported for each algorithm. The proposed KLA approach achieves the best minimum fitness value (1.2511) and the lowest average fitness value (1.2881). In addition, the SD of KLA (0.0258) is smaller than those of APO, PSO, and DE, which indicates more stable convergence behavior across independent trials. The competing methods produce higher mean fitness values, namely 1.3442 for APO, 1.4133 for PSO, and 1.3874 for DE, together with larger dispersions. To further assess statistical significance, pairwise comparisons were performed using the Wilcoxon signed-rank test [19]. The resulting p values, also listed in Table 3, are on the order of 10^{-5} when KLA is compared against each competing algorithm. These values are well below commonly accepted significance levels, indicating that the observed performance improvements of KLA are statistically meaningful rather than incidental.

The convergence characteristics of the algorithms are compared in Figure 7, where the average fitness evolution with respect to iteration number is presented. It can be seen that the KLA-based optimizer reduces the fitness value more rapidly during the early iterations and reaches a lower steady level than the alternative methods. APO shows a moderate convergence speed, whereas PSO and DE exhibit slower and more oscillatory convergence profiles. The faster descent and smoother stabilization observed for KLA suggest a more effective balance between exploration and exploitation during the search process.

The controller parameters corresponding to the best solutions found by each algorithm are listed in Table 4. Distinct parameter sets are obtained by different optimizers, yet the parameter vector produced by KLA yields the lowest objective value according to Equation (15). These optimized FOPID parameters are used in the subsequent time-domain and robustness analyses reported in the following subsections. Overall, the statistical results demonstrate that the proposed KLA-based tuning framework provides superior fitness performance, improved consistency, and faster convergence compared to APO, PSO, and DE under the same computational budget.

4.2 | Time Response Analysis

The time-domain behavior of the electro-hydraulic positioning system under the optimized FOPID controllers was examined using a unit step reference tracking corresponding to a 20 cm actuator displacement command. The FOPID parameters obtained by KLA, APO, PSO, and DE (Table 4) were individually applied to the same closed-loop plant model, and the resulting actuator displacement responses were compared. The comparative step responses are presented in Figure 8. It is observed that all optimized FOPID controllers are capable of stabilizing the actuator displacement and

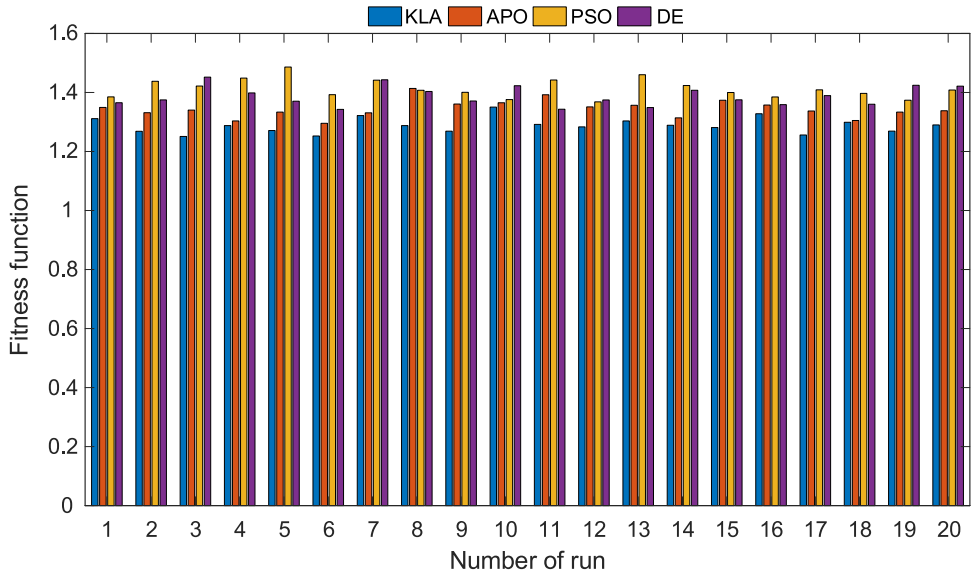


FIGURE 6 | Comparative fitness function evaluation with respect to the number of runs.

TABLE 3 | Results of the statistical analysis and nonparametric Wilcoxon's test.

Algorithm	Minimum	Maximum	Average	SD	p
KLA	1.2511	1.3504	1.2881	0.0258	–
APO	1.2956	1.4138	1.3442	0.0292	8.8575E−05
PSO	1.3682	1.4863	1.4133	0.0316	8.8575E−05
DE	1.3428	1.4521	1.3874	0.0327	8.8575E−05

27671402, 0, Downloaded from https://onlinelibrary.wiley.com/doi/10.1002/msd2.70076 by Turkey Cochrane Evidence Aid, Wiley Online Library on [04/09/2026]. See the Terms and Conditions (https://onlinelibrary.wiley.com/terms-and-conditions) on Wiley Online Library for rules of use; OA articles are governed by the applicable Creative Commons License

achieving accurate reference tracking without oscillatory instability. However, noticeable differences arise in the transient phase. The controller tuned by the proposed KLA method produces the fastest initial rise and reaches the reference level earlier than the alternatives. The APO- and DE-based designs follow closely, while the PSO-based controller exhibits a relatively slower approach to the setpoint. The enlarged inset shown in Figure 8 further highlights the early transient interval, where the separation between the response curves becomes more apparent.

A quantitative comparison of the main time-domain performance indicators is given in Table 5. The rise time t_r, settling time t_s (±2% band), OS, and IAE [38] are reported for each method. Among all candidates, the KLA-based FOPID controller achieves the smallest rise time (0.1664 s) and the shortest settling time (0.3034 s). The corresponding overshoot value is also the lowest (0.0124%), indicating a well-damped transient response. In addition, the IAE metric ($\mathrm{IAE} = \int_0^{t_{\mathrm{sim}}} |e(t)| \mathrm{d}t$), defined as the time integral of the absolute tracking error over the simulation horizon, attains its minimum value (1.5244 cm·sec) with the KLA-tuned controller. This result indicates superior overall error-suppression capability throughout the transient interval.

The competing optimizers yield slightly slower and less accurate responses. The APO-based design results in a rise time of 0.1777 s and a settling time of 0.3176 s, with higher overshoot and IAE values than those obtained with KLA. The PSO-based controller shows the slowest transient among the four, with both rise and settling times increased and the largest IAE value recorded. The DE-based tuning produces intermediate performance but remains inferior to the KLA-based design in all listed metrics. Overall, the time-response results demonstrate that the FOPID controller tuned by the proposed KLA framework provides faster tracking, lower overshoot, and reduced accumulated error compared to the same controller structure tuned by APO, PSO, and DE. These findings are consistent with the statistical and convergence advantages reported in Section 4.1 and confirm that the improved fitness values achieved by KLA translate directly into superior closed-loop transient performance.

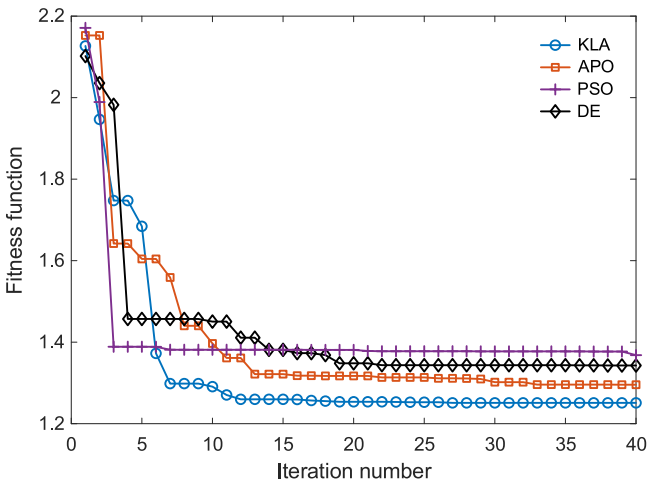


FIGURE 7 | Comparative convergence curves of KLA, APO, PSO, and DE.

4.3 | Comparison With Other Controllers

To further validate the effectiveness of the proposed KLA-based FOPID controller, additional comparative studies were conducted using several widely adopted controller structures. In this stage, a two-degree-of-freedom PID (2-DOF PID), a PID controller with derivative filter (PIDF), and a classical PI

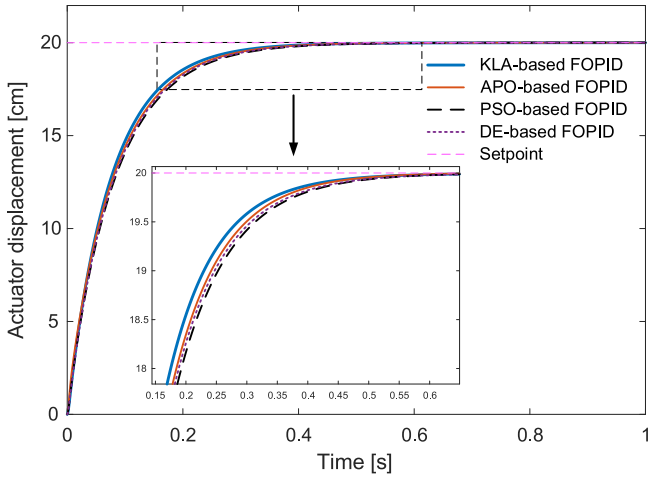


FIGURE 8 | Comparative step responses for the actuator displacement.

TABLE 5 | Comparison of most important stability metrics.

Algorithm	t_r [s]	t_s [s]	*OS* [%]	*IAE* [cm·s]
KLA	0.1664	0.3034	0.0124	1.5244
APO	0.1777	0.3176	0.0223	1.5771
PSO	0.1838	0.3337	0.0212	1.6659
DE	0.1792	0.3267	0.0170	1.6356

TABLE 4 | Optimal FOPID parameters obtained by KLA, APO, PSO, and DE.

Algorithm	K_p	K_i	K_d	λ	μ
KLA	0.039857	0.00019150	0.00036291	0.62736	0.53040
APO	0.038864	0.00013164	0.00021942	0.91264	0.89428
PSO	0.036476	0.00026835	0.00031938	0.54620	0.64082
DE	0.037081	0.00023813	0.00038326	0.58515	0.53892

27671402, 0, Downloaded from https://onlinelibrary.wiley.com/doi/10.1002/msd2.70076 by Turkey Cochrane Evidence Aid, Wiley Online Library on [04/09/2026]. See the Terms and Conditions (https://onlinelibrary.wiley.com/terms-and-conditions) on Wiley Online Library for rules of use; OA articles are governed by the applicable Creative Commons License

controller were considered. For a fair comparison, the optimal parameters of all competing controllers were obtained using the same KLA, the same objective function defined in Equation (15), and the same electro-hydraulic plant model and simulation conditions adopted for the FOPID controller. In this way, the influence of the tuning algorithm was kept identical for all controller structures, and the observed performance differences can therefore be attributed directly to the characteristics of the controller architectures themselves rather than to differences in the optimization procedure. The mathematical forms of the compared controllers are summarized as follows. The 2-DOF PID controller in the Laplace domain is expressed as [39]:

$$U(s) = K_p[\alpha R(s) - Y(s)] + \frac{K_i}{s}E(s) + \frac{K_d N s}{s+N}[\beta R(s) - Y(s)] \tag{15}$$

where α and β are setpoint weighting coefficients that enable separate shaping of reference tracking and disturbance rejection behavior. Through this structure, the proportional and derivative actions can be partially decoupled from the feedback signal, allowing improved transient shaping without excessively amplifying measurement noise. The PIDF is written as [40]:

$$U(s) = E(s)\left(K_p + \frac{K_i}{s} + \frac{K_d N s}{s+N}\right) \tag{16}$$

In this formulation, the derivative term is filtered by a first-order low-pass element. This filtering reduces high-frequency noise sensitivity while preserving the predictive action of the derivative component. Such a structure is frequently preferred in practical implementations where measurement noise cannot be neglected. For reference, the classical PI controller is given by [41]:

$$U(s) = E(s)\left(K_p + \frac{K_i}{s}\right) \tag{17}$$

This controller includes proportional and integral actions only and is commonly used due to its simple structure and ease of implementation, although its transient shaping capability is more limited compared to PID-type controllers.

The optimal controller parameters obtained through KLA tuning are listed in Table 6. It is observed that each controller type leads to a distinct optimal gain configuration. For the 2-DOF PID controller, additional parameters N, α, and β are also tuned, enabling extra flexibility in shaping the reference and feedback channels. The PIDF controller includes the derivative filter coefficient N, while the PI controller contains only proportional and integral gains.

The closed-loop step responses corresponding to the KLA-tuned controllers are presented in Figure 9 for the same actuator displacement setpoint used throughout the study. From the plotted responses, it is observed that all controllers achieve stable tracking; however, clear differences appear in the transient region. The FOPID controller reaches the reference level more rapidly and with a smoother trajectory. The 2-DOF PID and PIDF controllers exhibit slower rise behavior and more pronounced transient deviation from the setpoint. The PI controller shows the slowest approach among the compared methods, as expected due to the absence of derivative action and fractional dynamics.

A quantitative comparison based on standard time-domain performance indices is provided in Table 7. The reported metrics include rise time t_r, settling time t_s, OS, and IAE. According to Table 7, the KLA-based FOPID controller achieves the smallest rise time and settling time among all tested controllers. In addition, the overshoot level is significantly reduced compared to the integer-order alternatives. The IAE value is also the lowest for the FOPID case, indicating superior overall tracking accuracy across

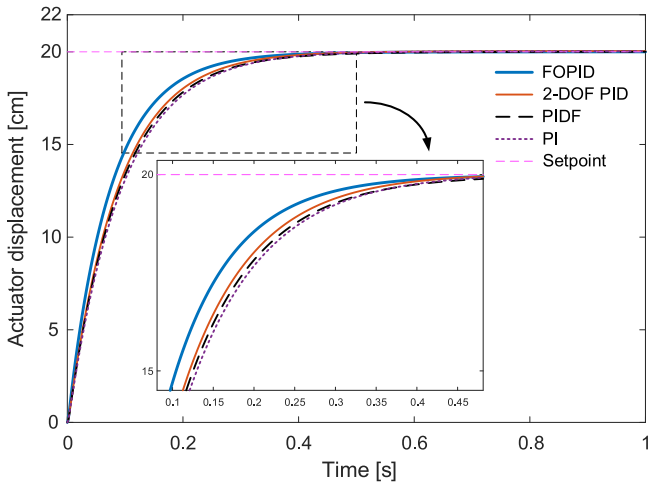


FIGURE 9 | Comparative step responses for the KLA based FOPID, 2-DOF PID, PIDF, and PI controllers.

TABLE 7 | Comparison of most important stability metrics for KLA-based FOPID, 2-DOF PID, PIDF, and PI controllers.

Controller type	t_r [s]	t_s [s]	*OS* [%]	*IAE* [cm·s]
FOPID	0.1664	0.3034	0.0124	1.5244
2-DOF PID	0.1886	0.3340	0.2142	1.7951
PIDF	0.1967	0.3554	0.0933	1.8378
PI	0.2024	0.3567	0.1797	1.9133

TABLE 6 | Optimal PI, PIDF, and 2-DOF PID parameters tuned by KLA.

Controller type	K_p	K_i	K_d	N	α	β
2-DOF PID	0.034191	0.00023058	0.00028072	2.2904	1.0016	1.1458
PIDF	0.033182	0.00038226	0.00033832	1.9736	—	—
PI	0.032540	0.00063274	—	—	—	—

27671402, 0, Downloaded from https://onlinelibrary.wiley.com/doi/10.1002/msd2.70076 by Turkey Cochrane Evidence Aid, Wiley Online Library on [04/09/2026]. See the Terms and Conditions (https://onlinelibrary.wiley.com/terms-and-conditions) on Wiley Online Library for rules of use; OA articles are governed by the applicable Creative Commons License

the full transient interval. The 2-DOF PID controller provides better performance than PIDF and PI in terms of overshoot reduction due to its setpoint weighting capability; however, it still remains inferior to the fractional-order design in both speed and accumulated error measures. The PIDF controller benefits from derivative filtering but exhibits longer settling behavior. The PI controller, while stable and smooth, produces the slowest transient and the highest error accumulation among the compared structures.

These results indicate that, under identical KLA-based tuning conditions, the fractional-order controller structure offers a broader and more effective tuning space for the considered electro-hydraulic positioning system. The additional fractional orders enable finer dynamic shaping, which translates into faster settling, lower overshoot, and reduced integral error. Therefore, the superiority of the proposed KLA-based FOPID controller over the KLA-tuned integer-order alternatives is confirmed both graphically in Figure 9 and numerically in Table 7.

5 | Robustness of Proposed KLA-Based FOPID Controller

In addition to the statistical and comparative results presented in Section 4, the robustness of the proposed KLA-based FOPID controller was further examined under more demanding operating conditions. The superiority of the proposed controller over the alternative optimizers and the KLA-tuned PI, PIDF, and 2-DOF PID controllers has already been established through the fair comparative analyses reported in Section 4. Therefore, the purpose of the present section is not to repeat the full structural comparison for every additional case study, but to further demonstrate that the proposed controller maintains its effectiveness under practically relevant non-ideal conditions, including variable reference trajectories, plant parameter variations, and simultaneous disturbance and measurement-noise effects. In this way, the results reported in this section complement the comparative findings of Section 4 and provide additional evidence of the practical robustness of the proposed method.

5.1 | Setpoint Tracking Analysis

In addition to unit-step regulation performance, the tracking capability of the proposed KLA-based FOPID controller was further examined under varying reference conditions. Since electro-hydraulic positioning systems frequently operate under changing command signals rather than fixed setpoints, it is necessary to verify that the designed controller preserves accuracy and stability when the reference trajectory varies over time. For this purpose, two different tracking scenarios were considered, and the actuator displacement responses were evaluated using the optimized KLA-based FOPID parameters obtained previously.

In the first scenario, a piecewise-constant variable setpoint profile was applied to the closed-loop system. The reference signal includes multiple level changes with both upward and downward steps. The corresponding actuator displacement response is shown in Figure 10. It is observed that the controller output follows each reference transition rapidly and smoothly. The actuator position converges to each new setpoint without noticeable oscillation or steady-state bias. During both increasing and decreasing transitions, the transient deviations remain small and quickly attenuate. No instability or sustained oscillatory behavior is observed throughout the full operating interval. These results indicate that the fractional-order control structure, together with KLA-based tuning, provides sufficient dynamic flexibility to handle multi-level reference commands within a single controller configuration.

A second tracking experiment was carried out using a continuously varying reference trajectory with sudden changes in slope and direction. This case represents a more demanding operating condition, where both fast variations and nonuniform reference segments are present. The corresponding tracking

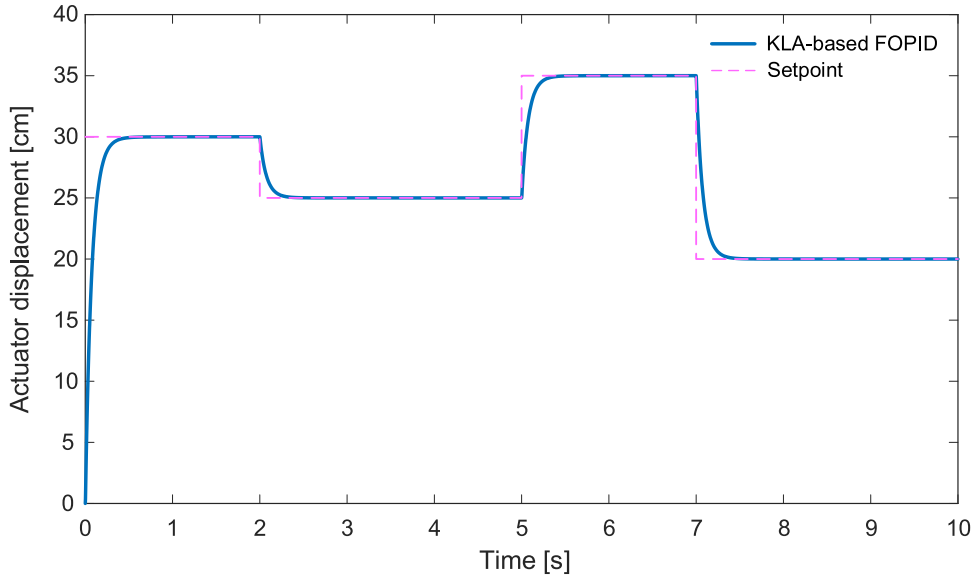


FIGURE 10 | Tracking performance of the KLA-based FOPID controller for the variable setpoint.

27671402, 0, Downloaded from https://onlinelibrary.wiley.com/doi/10.1002/msd2.70076 by Turkey Cochrane Evidence Aid, Wiley Online Library on [04/09/2026]. See the Terms and Conditions (https://onlinelibrary.wiley.com/terms-and-conditions) on Wiley Online Library for rules of use; OA articles are governed by the applicable Creative Commons License

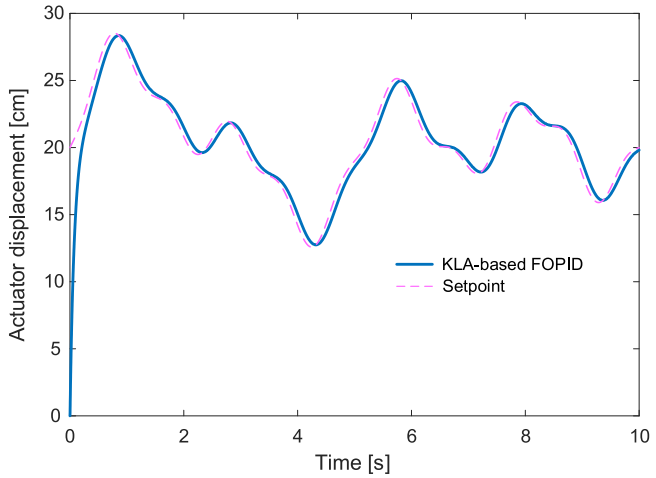


FIGURE 11 | Tracking performance of the KLA-based FOPID controller for the sudden changes in the setpoint.

response is presented in Figure 11. It can be seen that the actuator displacement closely follows the time-varying setpoint curve over the entire simulation horizon. Even in regions where abrupt changes occur, the tracking error remains limited and is rapidly corrected. The response curve remains smooth, and no excessive overshoot or high-frequency oscillation is introduced by the controller action. When Figures 10 and 11 are considered together, it is demonstrated that the KLA-based FOPID controller maintains consistent tracking quality for both multi-step and irregular reference profiles. The fractional integral and derivative orders provide additional tuning freedom, which enables better shaping of the dynamic response compared to integer-order structures. As a result, both transient deviation and accumulated tracking error are effectively reduced under variable setpoint conditions. These findings confirm that the proposed controller is not only effective for fixed-reference regulation but also robust and accurate in practical tracking applications involving changing command signals.

5.2 | Performance Analysis Under Parametric Changes

To further examine the robustness of the proposed KLA-based FOPID controller, a parametric sensitivity analysis was carried out by introducing structured variations into selected hydraulic system parameters. In practical electro-hydraulic systems, uncertainties and operating-condition changes may alter valve and actuator characteristics. Therefore, it is necessary to verify that the designed controller maintains acceptable performance when key plant parameters deviate from their nominal values. In this study, three parametric variation scenarios were defined based on the principal model coefficients introduced in Section 2. The following perturbations were considered:

- Scenario (I): the valve flow gain coefficient was decreased by 10% ($K_q = 0.359 \times 0.9 = 0.3231$)
- Scenario (II): the main spool feedback transducer gain was increased by 25% ($K_f = 1 \times 1.25 = 1.25$)
- Scenario (III): the effective actuator piston area was increased by 15% ($A = 1.1 \times 10^{-3} \times 1.15 = 1.265 \times 10^{-3}$)

These variations were selected to represent realistic deviations in valve flow characteristics, feedback scaling, and actuator geometry. For all scenarios, the controller parameters were kept fixed at the nominal KLA-optimized FOPID values, and only the plant parameters were modified. In this way, the intrinsic robustness of the controller could be evaluated without retuning.

The resulting step responses for nominal and perturbed cases are shown in Figure 12. It is observed that all perturbed scenarios remain stable and continue to track the 20 cm reference command successfully. Although slight differences in transient speed are visible, the overall response shapes remain close to the nominal curve. Scenario (II), corresponding to the increase in feedback gain, produces the slowest transient among the tested cases, while Scenario (I) yields a response closest to the nominal behavior. No oscillatory instability or divergence is observed in any scenario.

A quantitative comparison of the transient performance metrics under parametric variations is provided in Table 8. The nominal case results are included for reference. Under Scenario (I), the rise time and settling time increase moderately to 0.1847 and 0.3363 s, respectively, with only a small change in overshoot and IAE. Scenario (II) produces the largest degradation, where the rise time reaches 0.2093 s and the settling time increases to 0.3794 s. The IAE value also increases compared to nominal conditions. Scenario (III) leads to intermediate performance

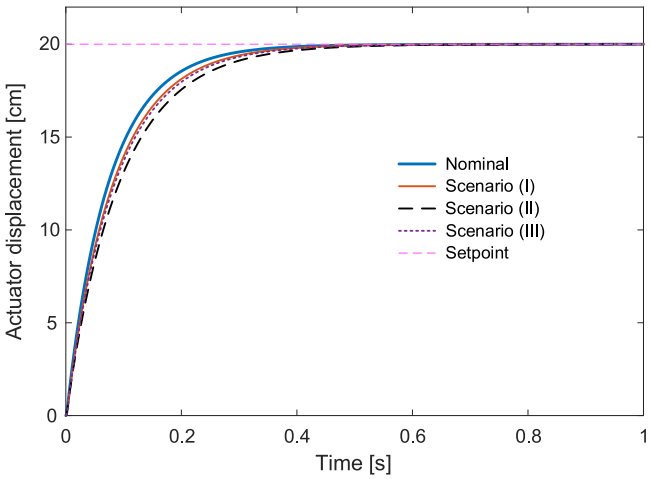


FIGURE 12 | Step response analysis for different scenarios of the parametric changes.

TABLE 8 | Performance of the KLA-based FOPID controller in terms of the most important stability metrics under parametric changes.

Scenario	t_r [s]	t_s [s]	*OS* [%]	*IAE* [cm·s]
Nominal	0.1664	0.3034	0.0124	1.5244
(I)	0.1847	0.3363	0.0138	1.6932
(II)	0.2093	0.3794	0.0154	1.9046
(III)	0.1917	0.3485	0.0142	1.7524

27671402, 0, Downloaded from https://onlinelibrary.wiley.com/doi/10.1002/msd2.70076 by Turkey Cochrane Evidence Aid, Wiley Online Library on [04/09/2026]. See the Terms and Conditions (https://onlinelibrary.wiley.com/terms-and-conditions) on Wiley Online Library for rules of use; OA articles are governed by the applicable Creative Commons License

changes, with metrics remaining between those of Scenarios (I) and (II).

Despite these variations, the OS remains very low in all cases, and the tracking error indices stay within a narrow and acceptable range. The limited spread of t_r, t_s, OS, and IAE values across all scenarios indicates that the closed-loop system performance is not highly sensitive to moderate parameter deviations. Overall, the results presented in Figure 12 and Table 8 demonstrate that the KLA-based FOPID controller preserves stability and satisfactory transient performance under representative plant parameter uncertainties. This behavior confirms that the proposed tuning approach yields a controller with strong parametric robustness for the considered electro-hydraulic positioning system.

5.3 | Performance Analysis Under External Disturbance and Noise Sources

In addition to parametric uncertainty and varying reference conditions, practical electro-hydraulic control systems are also affected by external disturbances and measurement noise. Such effects may originate from load variations, unmodeled hydraulic interactions, sensor imperfections, and electronic noise in the feedback channel. Therefore, an additional robustness study was conducted to evaluate the disturbance-rejection and noise-resilience capability of the proposed KLA-based FOPID controller. The disturbance and noise signals used in this analysis are illustrated in Figure 13. The external disturbance was modeled as a piecewise signal applied to the actuator channel, including both positive and negative step-like components with different magnitudes over time. This structure was selected to represent abrupt load changes and unexpected external influences acting on the mechanical subsystem. In parallel, measurement noise was introduced into the feedback signal as a zero-mean, rapidly varying random component with bounded amplitude. In this way, both process-side disturbance and sensor-side noise effects were represented simultaneously.

Using these inputs, the closed-loop system response obtained with the KLA-based FOPID controller is presented in Figure 14. It is observed that the actuator displacement initially reaches the setpoint with the same fast and well-damped transient behavior reported in previous sections. When the disturbance signal is applied, a temporary deviation from the reference value occurs; however, the controller compensates rapidly, and the output is driven back toward the setpoint within a short time interval. Similar behavior is observed at subsequent disturbance changes, where short-lived peaks appear but are quickly attenuated.

Despite the presence of continuous measurement noise, the output response remains smooth and tightly bounded around the reference level. No high-frequency oscillatory amplification is observed in the actuator displacement signal. This behavior indicates that the combined effect of the fractional-order structure and the optimized parameter set provides sufficient filtering and damping against noisy feedback components. The derivative action with fractional order contributes predictive behavior without introducing excessive noise sensitivity, while the fractional integral component supports steady-state accuracy during disturbance rejection. Overall, the results shown in Figures 13 and 14 demonstrate that the proposed KLA-based FOPID controller maintains stable operation, effective disturbance rejection, and strong noise tolerance under simultaneous disturbance and measurement noise conditions. Together with the parametric and tracking robustness results presented in Sections 5.1 and 5.2, these findings confirm that the designed controller provides reliable performance for the electro-hydraulic positioning system under realistic non-ideal operating environments.

6 | Conclusion

In this work, a KLA-based FOPID control framework has been presented for the position regulation of a two-stage electro-hydraulic actuator system. A control-oriented mathematical model was established from the linearized valve-flow relations, actuator continuity equation, and mechanical load dynamics, and a reduced second-order representation preserving the dominant system behavior was adopted for

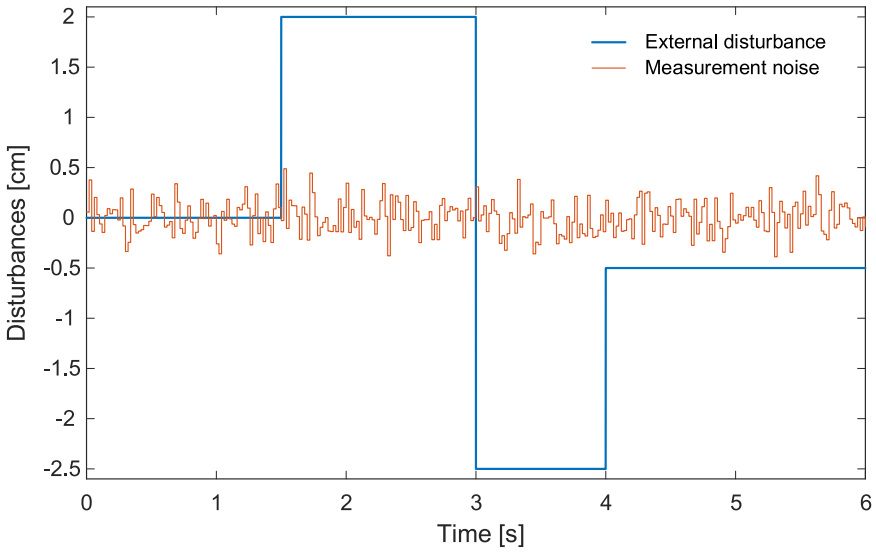


FIGURE 13 | The external disturbance and the measurement noise are considered for performance analysis of KLA-based FOPID controller.

27671402, 0, Downloaded from https://onlinelibrary.wiley.com/doi/10.1002/msd2.70076 by Turkey Cochrane Evidence Aid, Wiley Online Library on [04/09/2026]. See the Terms and Conditions (https://onlinelibrary.wiley.com/terms-and-conditions) on Wiley Online Library for rules of use; OA articles are governed by the applicable Creative Commons License

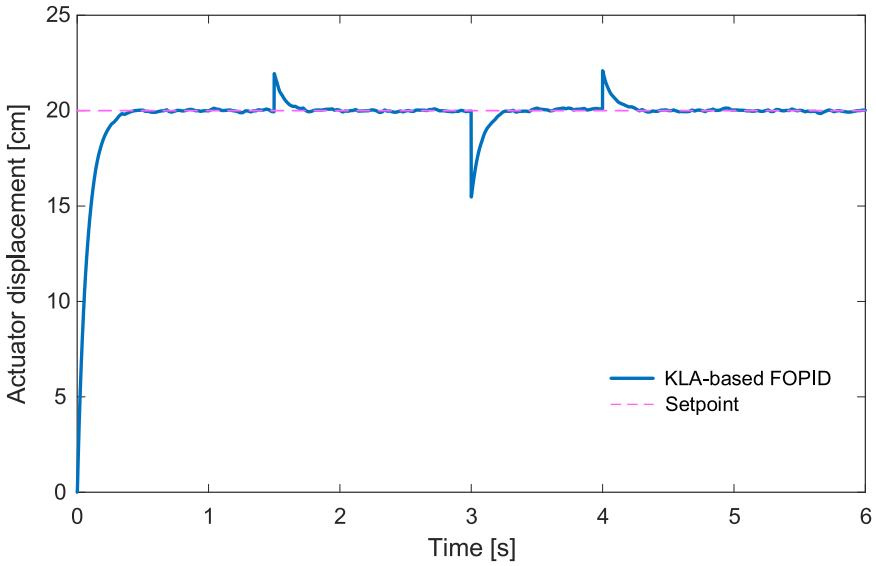


FIGURE 14 | Behavior of KLA-based FOPID controller in case of measurement noise and external disturbance.

controller design. On this basis, a FOPID controller structure was selected in order to enlarge the tuning space through fractional integral and derivative orders and thereby provide greater flexibility in shaping the closed-loop response than conventional integer-order controllers. The controller parameters were determined through an automatic tuning procedure formulated as a constrained optimization problem and solved by the KLA. The optimization task was defined through a composite time-domain objective function including OS, settling time, and integral error components. Under identical computational conditions and 20 independent runs, the proposed KLA approach produced the best statistical performance among the tested optimizers. More specifically, it achieved the lowest minimum fitness value of 1.2511, the lowest mean fitness value of 1.2881, and the smallest SD of 0.0258, while the statistical significance of the improvement was confirmed through Wilcoxon signed-rank tests against APO, PSO, and DE. The time-domain analyses further demonstrated that the KLA-tuned FOPID controller yielded the most favorable transient response among the compared designs. For a 20 cm step command, a rise time of 0.1664 s, a settling time of 0.3034 s, an overshoot of 0.0124%, and an IAE value of 1.5244 cm·s were obtained. In addition, when the comparison was extended to KLA-tuned PI, PIDF, and 2-DOF PID controllers, the proposed FOPID structure preserved its superiority in terms of response speed, damping quality, and accumulated tracking error. These findings indicate that the advantage of the proposed method is not limited to the optimizer itself, but is also associated with the structural flexibility introduced by the fractional-order controller formulation. The robustness investigations showed that the proposed controller maintained stable and accurate operation under variable and multi-level reference profiles, structured plant parameter changes from −10% to +25%, and simultaneous external disturbance and measurement-noise conditions. Although moderate performance degradation was observed under perturbed cases, low-overshoot behavior and closed-loop stability were preserved, and disturbance-induced deviations were rapidly attenuated without visible noise amplification in the actuator response. These results confirm that the proposed KLA-based FOPID controller is not only effective under nominal conditions but also reliable under practically relevant non-ideal operating scenarios.

As a natural continuation of the present study, future investigations may also address implementation-oriented aspects of the proposed control framework, including the computational complexity of the KLA-based tuning procedure, the practical tunability of the controller parameters, and the real-time feasibility of the fractional-order controller realization in embedded electro-hydraulic applications. In particular, experimental studies on a real-time electro-hydraulic platform would provide a suitable basis for evaluating execution burden, implementation constraints, and hardware-level applicability under practical operating conditions.

Conflicts of Interest

The authors declare no conflicts of interest.

Data Availability Statement

All data supporting the findings of this study are included within the manuscript.

References

1. W. M. Bessa, M. S. Dutra, and E. Kreuzer, "An Adaptive Fuzzy Dead-Zone Compensation Scheme and Its Application to Electro-Hydraulic Systems," *Journal of the Brazilian Society of Mechanical Sciences and Engineering* 32 (2010): 1–7, https://doi.org/10.1590/S1678-58782010000100001.

2. A. Plummer, "A General Co-Ordinate Transformation Framework for Multi-Axis Motion Control With Applications in the Testing Industry," *Control Engineering Practice* 18 (2010): 598–607, https://doi.org/10.1016/j.conengprac.2010.02.015.

3. K. Mehmood, N. I. Chaudhary, Z. A. Khan, et al., "Atomic Physics-Inspired Atom Search Optimization Heuristics Integrated With Chaotic Maps for Identification of Electro-Hydraulic Actuator Systems," *Modern Physics Letters B* 38 (2024): 2450308, https://doi.org/10.1142/S0217984924503081.

27671402, 0, Downloaded from https://onlinelibrary.wiley.com/doi/10.1002/msd2.70076 by Turkey Cochrane Evidence Aid, Wiley Online Library on [04/09/2026]. See the Terms and Conditions (https://onlinelibrary.wiley.com/terms-and-conditions) on Wiley Online Library for rules of use; OA articles are governed by the applicable Creative Commons License

4. B. Li, S. Riaz, O. Saleem, et al., "PD-Type Iterative Learning Consensus Control Approach for an Electromechanical Actuator-Based Multiagent System," *Applied Intelligence* 55 (2025): 684, https://doi.org/10.1007/s10489-025-06559-2.

5. J. Zhang, D. Cheng, Y. Liu, and G. Zhu, "Adaptive Fuzzy Sliding Mode Control for Missile Electro-hydraulic Servo Mechanism," in *7th World Congress on Intelligent Control and Automation* (IEEE, 2008), 5197–5202.

6. T. G. Ling, M. F. Rahmat, and A. R. Husain, "ANFIS Modeling of Electro-Hydraulic Actuator System Through Physical Modeling and FCM Gap Statistic in Initial FIS Determination," *Journal of Intelligent & Fuzzy Systems* 27 (2014): 1743–1755, https://doi.org/10.3233/IFS-141140.

7. Y. Xiao, C. Sun, and C. Lian, "Research on Tracking and Synchronization Control of Dual Hydraulic Cylinders Based on Improved Active Disturbance Rejection Control," *Engineering Research Express* 6 (2024): 035513, https://doi.org/10.1088/2631-8695/ad5c2b.

8. O. Saleem, M. Kazim, and J. Iqbal, "Robust Position Control of VTOL UAVs Using a Linear Quadratic Rate-Varying Integral Tracker: Design and Validation," *Drones* 9 (2025): 73, https://doi.org/10.3390/drones9010073.

9. Q. Chen, H. Sun, N. Wang, et al., "Sliding Mode Control of Hydraulic Pressure in Electro-Hydraulic Brake System Based on the Linearization of Higher-Order Model," *Fluid Dynamics & Materials Processing* 16 (2020): 513–524, https://doi.org/10.32604/fdmp.2020.09375.

10. S. Zaare and M. R. Soltanpour, "Optimal Robust Adaptive Fuzzy Backstepping Control of Electro-Hydraulic Servo Position System," *Transactions of the Institute of Measurement and Control* 44 (2022): 1247–1262, https://doi.org/10.1177/01423312211051496.

11. F. Haouari, R. Gouri, N. Bali, et al., "Performance Enhancement of Electrohydraulic Servo System Using Teaching Learning-Based Optimization and CDM-Backstepping With Disturbance Observer," *Journal of Control, Automation and Electrical Systems* 31 (2020): 926–934, https://doi.org/10.1007/s40313-020-00602-y.

12. J. Bhookya and R. K. Jatoth, "Optimal FOPID/PID Controller Parameters Tuning for the AVR System Based on Sine–Cosine-Algorithm," *Evolutionary Intelligence* 12 (2019): 725–733, https://doi.org/10.1007/s12065-019-00290-x.

13. M. F. Ghani, M. S. Hanaffi, M. H. I. Ishak, et al., "Simulation Evaluation of Electro-Hydraulic Tracking Performance Using an Optimized Fractional Order PID Controller," in *IEEE 8th International Conference on Electrical, Control and Computer Engineering* (IEEE, 2025), 188–192.

14. C. Chee Soon, R. Ghazali, S. Horng Chong, et al., "Comparison of Fractional Order PID Controller and Sliding Mode Controller With Computational Tuning Algorithm," *Universal Journal of Electrical and Electronic Engineering* 6 (2019): 181–190, https://doi.org/10.13189/ujeee.2019.060401.

15. D. Izci, S. Ekinci, M. Z. Mohd Tumari, and M. A. Ahmad, "A Novel Softsign Fractional-Order Controller Optimized by an Intelligent Nature-Inspired Algorithm for Magnetic Levitation Control," *Fractal and Fractional* 9 (2025): 801, https://doi.org/10.3390/fractalfract9120801.

16. A. K. Sahin, B. Cavdar, and M. S. Ayas, "An Adaptive Fractional Controller Design for Automatic Voltage Regulator System: Sigmoid-Based Fractional-Order PID Controller," *Neural Computing & Applications* 36 (2024): 14409–14431, https://doi.org/10.1007/s00521-024-09816-6.

17. S. Yang, Y. Li, D. Shi, and B. Yan, "Key Parameter Identification for Elevation Equilibrator Electro-Hydraulic System Based on Improved PSOA," in *7th International Conference on Advanced Algorithms and Control Engineering (ICAACE)* (IEEE, 2024), 1319–1323.

18. K. Mehmood, N. I. Chaudhary, Z. A. Khan, et al., "Design of Chaos Induced Aquila Optimizer for Parameter Estimation of Electro-Hydraulic Control System," *Computer Modeling in Engineering & Sciences* 143 (2025): 1809–1841, https://doi.org/10.32604/cmes.2025.064900.

19. D. Izci, E. Eker, S. Ekinci, et al., "Neighborhood Centroid Opposition-Based Flood Algorithm for Optimizing Fractional-Order PID Control in Nonlinear Heat Exchanger Dynamics," *Chaos, Solitons, and Fractals* 204 (2026): 117729, https://doi.org/10.1016/j.chaos.2025.117729.

20. D. Izci, F. Artun, S. Ekinci, et al., "Enhanced Hiking Optimization Algorithm for Robust PID Control in Doubly-Fed Induction Generator Systems for Wind Energy Applications," *IET Control Theory & Applications* 19 (2025): e70071, https://doi.org/10.1049/cth2.70071.

21. H. Feng, Y. Zhong, C. Zhou, et al., "Collaborative High-Precision Trajectory Control for Heavy Excavators Based on an Improved Particle Swarm Optimization Algorithm," *Automation in Construction* 180 (2025): 106546, https://doi.org/10.1016/j.autcon.2025.106546.

22. W. Ma, S. Ma, W. Qiao, et al., "Research on PID Controller of Excavator Electro-Hydraulic System Based on Improved Differential Evolution," *Machines* 11 (2023): 143, https://doi.org/10.3390/machines11020143.

23. D. Izci, S. Ekinci, M. Jabari, et al., "A Novel Gudermannian Function-Driven Controller Architecture Optimized by Starfish Optimizer for Superior Transient Performance of Automatic Voltage Regulation," *Biomimetics* 11 (2025): 7, https://doi.org/10.3390/biomimetics11010007.

24. S. Saat, M. A. Ahmad, and M. R. Ghazali, "Data-Driven Brain Emotional Learning-Based Intelligent Controller-PID Control of Mimo Systems Based on a Modified Safe Experimentation Dynamics Algorithm," *International Journal of Cognitive Computing in Engineering* 6 (2025): 74–99, https://doi.org/10.1016/j.ijcce.2024.11.005.

25. Z. Li, Z. Guan, T. Yamamoto, and S. Omatu, "Realization of a Database-Driven PID Control System Using a CMAC Memory," *Electronics and Communications in Japan* 106 (2023): 281–288, https://doi.org/10.1002/ecj.12406.

26. M. R. Ghazali, M. A. Ahmad, R. M. T. Raja Ismail, and M. O. Tokhi, "An Improved Neuroendocrine–Proportional–Integral–Derivative Controller With Sigmoid-Based Secretion Rate for Nonlinear Multi-Input–Multi-Output Crane Systems," *Journal of Low Frequency Noise, Vibration and Active Control* 39 (2020): 1172–1186, https://doi.org/10.1177/1461348419867524.

27. M. Ghasemi, N. Khodadadi, P. Trojovský, et al., "Kirchhoff's Law Algorithm (KLA): A Novel Physics-Inspired Non-Parametric Metaheuristic Algorithm for Optimization Problems," *Artificial Intelligence Review* 58 (2025): 325, https://doi.org/10.1007/s10462-025-11289-5.

28. X. Wang, V. Snášel, S. Mirjalili, et al., "Artificial Protozoa Optimizer (APO): A Novel Bio-Inspired Metaheuristic Algorithm for Engineering Optimization," *Knowledge-Based Systems* 295 (2024): 111737, https://doi.org/10.1016/j.knosys.2024.111737.

29. A. G. Gad, "Particle Swarm Optimization Algorithm and Its Applications: A Systematic Review," *Archives of Computational Methods in Engineering* 29 (2022): 2531–2561, https://doi.org/10.1007/s11831-021-09694-4.

30. K. V. Price, "Differential Evolution," In: *Handbook of Optimization. Intelligent Systems Reference Library*, vol. 38, ed. I. Zelinka, V. Snášel, and A. Abraham (Springer, 2013), https://doi.org/10.1007/978-3-642-30504-7_8.

31. V. K. Singh, S. Sharma, and P. K. Padhy, "Controlling of AVR Voltage and Speed of DC Motor using Modified PI-PD Controller," in *2nd IEEE International Conference on Power Electronics, Intelligent Control and Energy Systems (ICPEICES)* (IEEE, 2018), 858–863.

32. B. Ebrahimi, R. Tafreshi, H. Masudi, et al., "A Parameter-Varying Filtered PID Strategy for Air–Fuel Ratio Control of Spark Ignition Engines," *Control Engineering Practice* 20 (2012): 805–815, https://doi.org/10.1016/j.conengprac.2012.04.001.

27671402, 0, Downloaded from https://onlinelibrary.wiley.com/doi/10.1002/msd2.70076 by Turkey Cochrane Evidence Aid, Wiley Online Library on [04/09/2026]. See the Terms and Conditions (https://onlinelibrary.wiley.com/terms-and-conditions) on Wiley Online Library for rules of use; OA articles are governed by the applicable Creative Commons License

33. C. Turkeri, S. Ekinci, D. Izci, and O. Kiselychnyk, "FGO-Tuned 2-DOF PI Controller for Pressure Regulation in Centrifugal Fans Driven by Induction Motors Using an Experimentally Validated Model," *ISA Transactions* 169 (2026): 436–446, https://doi.org/10.1016/j.isatra.2025.12.012.

34. F. Golnaraghi and B. C. Kuo, *Automatic Control Systems*, 8th ed. (McGraw-Hill Education, 2017).

35. N. D. Manring and R. C. Fales, *Hydraulic Control Systems* (Wiley, 2019).

36. S. Tufenkci, B. Senol, B. B. Alagoz, and R. Matušů, "Disturbance Rejection FOPID Controller Design in V-Domain," *Journal of Advanced Research* 25 (2020): 171–180, https://doi.org/10.1016/j.jare.2020.03.002.

37. D. Izci and S. Ekinci, "A Novel-Enhanced Metaheuristic Algorithm for FOPID-Controlled and Bode's Ideal Transfer Function–Based Buck Converter System," *Transactions of the Institute of Measurement and Control* 45 (2023): 1854–1872, https://doi.org/10.1177/01423312221140671.

38. D. Izci, S. Ekinci, E. Çelik, et al., "Design of Novel Exponential PDN Controller via Quadratic Interpolation Optimiser for Nonlinear and Unstable Ball and Beam System," *IET Control Theory & Applications* 20 (2026): e70107, https://doi.org/10.1049/cth2.70107.

39. S. Ekinci, D. Izci, M. Jabari, et al., "Nonlinear 2-DOF PID Controller Optimized by Artificial Lemming Algorithm for Robust Engine Speed Regulation in Spark-Ignition Systems," *Scientific Reports* 15 (2025): 44264, https://doi.org/10.1038/s41598-025-27873-2.

40. S. Ekinci, D. Izci, C. Turkeri, et al., "Flood Algorithm-Tuned PID-F Controller With a Modified Objective Function for Robust and Noise-Resilient Speed Control of Nonlinear Sparkignition Engines," *Scientific Reports* 15 (2025): 45481, https://doi.org/10.1038/s41598-025-29231-8.

41. S. Ekinci, C. Turkeri, D. Izci, et al., "Optimizing Steam Condenser Efficiency: Integrating Logarithmic Spiral Search and Greedy Selection Mechanisms in Gazelle Optimizer for PI Controller Tuning," *Results in Engineering* 24 (2024): 103501, https://doi.org/10.1016/j.rineng.2024.103501.

27671402, 0, Downloaded from https://onlinelibrary.wiley.com/doi/10.1002/msd2.70076 by Turkey Cochrane Evidence Aid, Wiley Online Library on [04/09/2026]. See the Terms and Conditions (https://onlinelibrary.wiley.com/terms-and-conditions) on Wiley Online Library for rules of use; OA articles are governed by the applicable Creative Commons License